NANO LETTERS

pubs.acs.org/NanoLett Letter

# Tunable, Ferroelectricity-Inducing, Spin-Spiral Magnetic Ordering in Monolayer FeOCl

De-Liang Bao,[‖] Andrew O'Hara,[‖] Shixuan Du, and Sokrates T. Pantelides*

Cite This: *Nano Lett.* 2022, 22, 3598−3603 Read Online

ACCESS | Metrics & More | Article Recommendations | Supporting Information

**ABSTRACT:** Spin spirals (SS) are a special case of noncollinear magnetism, where the magnetic-moment direction rotates along an axis. They have generated interest for novel phenomena, spintronics applications, and their potential formation in monolayers, but the search for monolayers exhibiting SS has not been particularly fruitful. Here, we employ density functional theory calculations to demonstrate that SS form in a recently synthesized monolayer, FeOCl. The SS wavelength and stability can be tuned by doping and uniaxial strain. The SS-state band gap is larger by 0.6 eV compared to the gap of both the ferromagnetic and antiferromagnetic state, enabling bandgap tuning and possibly an unusual formation of quantum wells in a single material via magnetic-field manipulation. The SS-induced out-of-plane ferroelectricity enables switching of the SS chirality by an electric field. Finally, forming heterostructures, for example, with graphene or boron nitride, maintains SS ordering and provides another method of modulation and a potential for magnetoelectric devices.

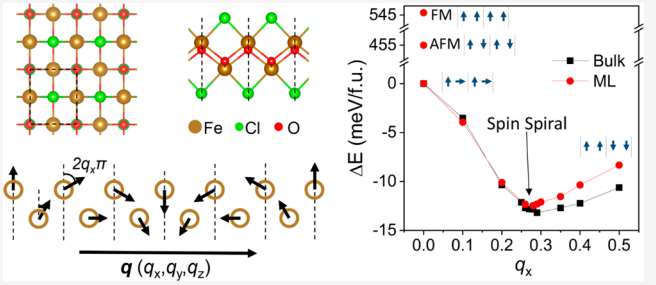


**KEYWORDS:** *monolayer, spin spiral, ferroelectricity, type-II multiferroic, bandgap engineering*



Materials and nanostructures exhibiting noncollinear magnetism, especially spin spirals (SS), have attracted interest because of the diverse phenomena that can be realized.[1−5] Such materials are characterized by an unusual multiferroic behavior: The SS state spontaneously breaks both time-reversal and inversion symmetries, which induces non-displacive ferroelectricity and a nonlinear interaction between magnetism ($M$) and electric polarization ($P$).[6−9] The polarization direction is a complex function of the noncollinear spins.[8] Therefore, since the magnetism and ferroelectricity in these materials are inherently coupled (type-II multiferroicity), one expects large magnetoelectric effects, that is, the ability to control each property by an external field of the other type, especially the ability to switch the polarization using weak magnetic fields.[10,11] These properties offer more flexibility for the development of novel spintronics devices and related technology.[12,13]

In order to realize useful SS features, the ability to control and tune SS ordering would be beneficial but remains challenging. In the case of transition-metal films on surfaces, researchers have found that SS can be manipulated through intercalation, temperature, and strain.[14−17] Adjusting the interatomic distance in iron atomic chains[18] enables tuning of the SS period. Considering that two-dimensional (2D) monolayer materials possess advantages in heterostructure fabrication, strain engineering, electrostatic doping, and functionalization, the realization of SS with tailored ferroelectric properties in 2D monolayers provides an attractive prospect for spintronic nanodevices. Recently, monolayer $NiI_2$ has attracted attention due to its unique magnetic ordering, but the mechanism of its helimagnetism remains elusive as it may be due to the combination of short-range symmetric exchange and magnetic frustration[19] or long-range magnetic exchange interactions.[20] SS have been predicted to exist in other monolayers such as $MnCl_2$,[21] $VOI_2$,[22] $Fe_3GeTe_2$,[23] and $Hf_2VC_2F_2$,[24] but so far the effect of SS on the electronic structure, for example, band gaps, or, conversely, the effect of strain or chemical doping on the SS have not been investigated.

So far, the monolayers that have been predicted to host SS ordering have not been fabricated and no experiments have found monolayers that host SS ordering. A natural place to look for monolayers that have been fabricated and are likely to host SS ordering is in layered, van der Waals (vdW) materials that are known to feature SS ordering in their bulk form. One such material is FeOCl.[25,26] FeOCl was successfully exfoliated down to ultrathin nanosheets, possibly bilayers, in 2020.[27] The presence of SS ordering was not explored either by experiments or theory, but a low-temperature transition was detected in the magnetic susceptibility, indicative of canted

**Received:** December 31, 2021
**Revised:** April 15, 2022
**Published:** April 22, 2022

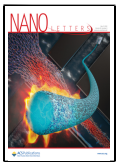





https://doi.org/10.1021/acs.nanolett.1c05043
*Nano Lett.* 2022, 22, 3598−3603

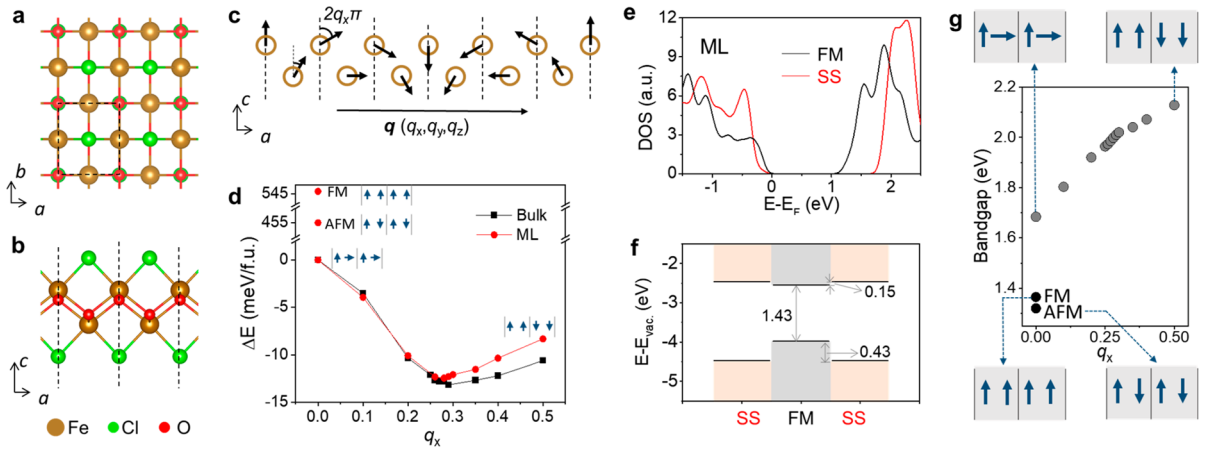


**Figure 1.** Atomic structure, spin-spiral magnetic ordering, and density of states in ML FeOCl. (a) Top view of ML FeOCl showing the *ab* plane. (b) Side view of ML FeOCl showing the *ac* plane. (c) Schematic of spin-spiral magnetic ordering in ML FeOCl with a propagation vector $q$ in the *a* direction ($q_x$ = 1/6). Only magnetic Fe atoms (brown circles) are shown for visual clarity. Black arrows indicate the directions of the noncollinear magnetic moments. Coordinates *x*, *y*, and *z* correspond to directions along the *a*, *b*, and *c* lattice vectors, respectively. (d) The relative energies of bulk (black curve) and ML (red curve) FeOCl as a function of $q_x$. In each case, the energy of the state $q_x$ = 0 is set to zero. The schematics with the blue arrows indicate the spin orderings of the $q_x$ = 0 and $q_x$ = 0.5 SS states and of the higher-energy standard FM and AFM states. The pairs of arrows in each unit cell designate the spins of the Fe atoms in the two sublattices. (e) DOS plots of ML FeOCl in the FM (black curves) and SS (red curves) states, respectively. (f) Schematic of the proposed quantum well based on the effect of different magnetic orderings on the energy gap. The band offsets are in eV. (g) Bandgap evolution as a function of the SS $q_x$ of ML FeOCl. Four schematics as in (d) are used to illustrate the distinct $q_x$ = 0, $q_x$ = 0.5, FM, and AFM states.

magnetism. In 2019, however, monolayer FeOCl was successfully synthesized by electron irradiation of an $FeCl_3$ monolayer intercalated in bilayer graphene.[28]

In this paper, we report the discovery of SS multiferroicity in monolayer (ML) FeOCl using density-functional-theory (DFT) calculations. We found that in freestanding ML FeOCl cycloidal SS magnetic ordering is the magnetic-ordering ground state, as is the case in bulk FeOCl, with a propagation vector of (0.277, 0.5, 0). We confirmed the SS ground state by comparing the Heisenberg exchange ($J$) and the Dzyaloshinskii−Moriya interaction ($D$). SS ordering leads to an increase in the band gap of ML FeOCl by ∼0.6 eV relative to either the ferromagnetic (FM) or antiferromagnetic (AFM) states, which can potentially lead to an unusual transistor design. The SS propagation vector is tunable by either *n*-type or *p*-type doping and by uniaxial strain. Numerically, the SS period changes linearly with doping concentration. Furthermore, the SS generate an out-of-plane electrical polarization (ferroelectricity) in ML FeOCl without atomic displacements. Reversal of the SS's chirality inverts the polarization, whereby the SS chirality can be controlled by an electric field. Plotting of the charge-density difference between the ferromagnetic state and the SS state reveals that the electrons redistribute asymmetrically in the *z*-direction, confirming that the magnetic ordering is the source of the electronic polarization. Lastly, in an encapsulating heterostructure where the ML FeOCl is sandwiched between graphene monolayers, as in the experiments of ref 28, the FeOCl becomes doped *n*-type and the SS propagation vector is correspondingly shortened. For ML FeOCl encapsulated by h-BN, the *d* orbitals of Fe are redistributed resulting in a SS state with a shorter propagation vector. Given the above and the fact that FeOCl has already been fabricated by intercalation within bilayer graphene, there are possibilities for the design of magnetoelectric devices fabricated via intercalation, for example, as proposed in ref 29, for ferroelectric devices based on monolayers and heterostructures.

We first employed DFT calculations to confirm that freestanding ML FeOCl is stable (in the FM, AFM, and SS magnetic orderings, there are no imaginary-frequency phonon modes; see Supporting Information). The atomic structure of ML FeOCl with $a$ = 3.20 Å and $b$ = 3.81 Å, and space group *Pmmn* (No. 59) is shown in Figure 1a,b. On the basis of the SS ordering in bulk FeOCl,[25,26] we investigated SS ordering in ML FeOCl as shown in Figure 1c. The SS generated by Fe-atom magnetic moments lie in the *ac* plane and propagate along the *a*-direction forming a cycloidal SS. The normalized propagation vector $q$ (per unit cell, so that $2\pi q$ is measured in radians) characterizes both the direction and period of the SS ordering. The normalized numerical values of $q$ vary from 0 to 0.5, while any other value corresponds to a gradually rotating spin ordering, that is, an SS (negative values or values between 0.5 and 1.0 represent a reverse chirality). In the present case, we confine $q_y$ and $q_z$ as constants with $q_y$ = 0.5 (same as the bulk, AFM coupling along the *b*-axis; we checked that no SS forms along the *b*-direction; see Figure S4) and $q_z$ = 0 (corresponding to no ordering along the *z*-axis due to the monolayer limit). Thus, we only need to consider optimization of $q_x$ as shown in Figure 1d. The total energy of bulk and ML FeOCl show minima at $q_x$ = 0.291 and $q_x$ = 0.274, respectively, demonstrating SS ground states in both cases. It is noteworthy that the $q_x$ = 0 and $q_x$ = 0.5 states in ML FeOCl do not correspond to standard FM or AFM orderings because there are two Fe sublattice. Instead, in the $q_x$ = 0 state the magnetic moments of Fe atoms in the first sublattice point in the *c*-direction while those of the Fe atoms in the second sublattice point in the *a*-direction, standard FM and AFM states have higher energies, 545 and 455 meV/f.u., respectively, than the $q_x$ = 0 state, that is, the SS state is the ground state. We considered other SS orderings that propagate along *a* but rotate in the *ab* or *bc* planes and found that the energies are higher by 47.6 and 30.1 meV/Fe atom relative to the SS in the *ac* plane, respectively.



https://doi.org/10.1021/acs.nanolett.1c05043
Nano Lett. 2022, 22, 3598−3603

The minor discrepancy between the calculated bulk $q_x$ and the previously reported experimental $q_x$ (0.275 or 2/7)[25,26] is attributed to other effects such as strain and doping, that will be discussed later. We further confirmed the SS ground state of ML FeOCl by calculating and comparing the Heisenberg exchange ($J$) and Dzyaloshinskii−Moriya ($D$) interactions. We found that $\mathbf{J}$ is relatively close to $D$ in the $a$-direction while $\boldsymbol{J}$ dominates in the $b$-direction, which are consistent with the calculated spin structure (see details in the Supporting Information). By proposing a simple one-dimensional model, we estimated the quantitative relationship between directional magnetic ordering and variable $\boldsymbol{J}-\boldsymbol{D}$ interactions (see details in Supporting Information). The single-ion anisotropies (SIA) are $A_{ii}^{zz} - A_{ii}^{xx} = -0.020$ meV/Fe atom and $A_{ii}^{yy} - A_{ii}^{xx} = 0.012$ meV/Fe atom, while the total magnetocrystalline-anisotropy energies (MAEs) of $a \rightarrow b$ and $c \rightarrow b$ are −0.028 and −0.082 meV/Fe atom, respectively.

The band gap of ML FeOCl is found to be highly dependent on magnetic ordering. The density of states (DOS) of ML FeOCl with FM and SS orderings are shown in Figures 1e. The band gap is widened by ∼0.6 eV from the FM state to the SS state. Because of the local-density-approximation (LDA) exchange-correlation functional used in this work, the bandgaps in Figure 1e are underestimated, while the relative change of the bandgaps is reliable (previously, using a hybrid exchange functional, we reported that ML FeOCl has similar bandgaps in the AFM (∼2.5 eV) and FM (∼2.7 eV) phases[28]). The large difference in the bandgaps of the FM and SS states affects both the electronic and optical properties, making ML FeOCl a candidate for future magnetoelectric or magneto-optical devices. In particular, one can envision FeOCl-based quantum wells formed in a monolithic material as shown schematically in Figure 1f. In principle, the manipulation of the magnetic orderings to form the quantum well can be done either using a magnetic field or using an electric field by using a multiferroic layer or special magnetoelectric heterostructures.[30−32] The bandgap of ML FeOCl is found to change approximately linearly with $q_x$, while the bandgaps of FM/AFM ML FeOCl are smaller (Figure 1g).

The SS states in ML FeOCl are highly sensitive to tuning by electrostatic doping (in calculations the doping is achieved by adding or removing fractional electrons from the calculational cells; the charge is automatically compensated by a uniform background charge of the opposite sign). Figure 2a shows the evolution of $q_x$ as the type and density of doping are changing. Note that $n$-type doping causes a decrease of $q_x$, which means a longer SS period, while $p$-type doping causes an increase of $q_x$, which means a shorter SS period. Figure 2a also shows that $n$-type doping at levels larger than $\sim 5 \times 10^{13}$ cm$^{-2}$ reverse the relative stability of the $q_x = 0$ and $q_x = 0.5$ states. In the undoped and low-density $n$-type doping cases, $q_x = 0.5$ ordering is more stable, while with strong $n$-type doping $q_x = 0$ becomes more stable. On the other hand, in $p$-typed doping, the $q_x = 0.5$ state is always more stable than the $q_x = 0$ state. The linear relationship between $q_x$ and doping density is extracted and shown in Figure 2b.

Two-dimensional materials are also highly susceptible to strain tunability with several practical methods existing to implement strain engineering.[33] To analyze the SS's sensitivity to uniaxial strain, we consider compressive and tensile strain along the $a$ direction of FeOCl, parallel to the spiral propagation direction. As shown in Figure 2c, uniaxial strain tunes the SS propagation vector in a monotonic fashion, that

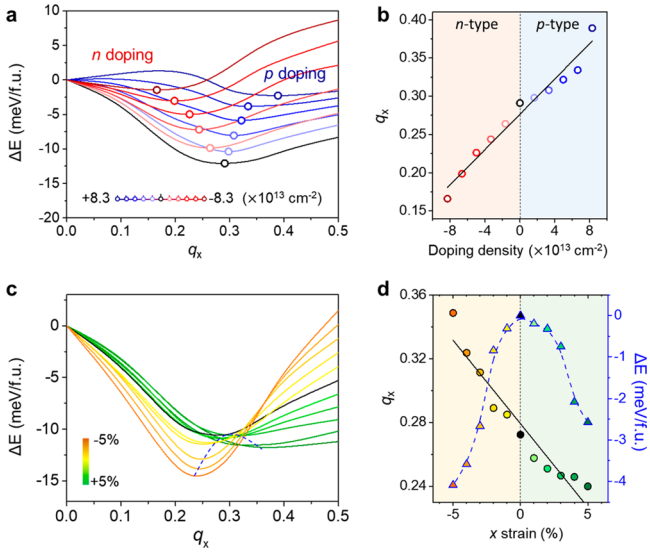


**Figure 2.** Tunability of SS in ML FeOCl. (a) Effects of electron/hole doping on SS states. The doping densities range between 0 and 8.3 × $10^{13}$ cm$^{-2}$ ($n$-type densities are shown in red and $p$-type densities are shown in blue). Open circles mark the SS ground states at different doping densities. At each doping density, the $q_x = 0$ energy is set to 0. (b) Linear relationship between $q_x$ and doping densities, extracted from panel a. (c) Effects of uniaxial strain on SS states. The uniaxial strain is along the $a$ lattice direction (i.e., $q_x$ direction) and varies in the range ±5%. At each strain state, the $q_x = 0$ energy is set to 0. Orange/green colors indicate compression/expansion, respectively. (d) The linear relationship between $q_x$ and strain (black circles and line), and the parabolic relationship between relative energies (the energy difference between SS and $q_x = 0$ states at each strain state) and strain (blue open triangles and dashed curve). The unstrained SS energy is set to 0.

is, compressive strain decreases $q_x$, while tensile strain increases $q_x$. Thus, $a$-direction compressive strain lengthens the SS period while $a$-direction tensile strain shortens it. The modulation of $q_x$ with strain is approximately linear (black line in Figure 2d). For either compressive or tensile strain, the SS-state energy is lowered even further relative to the $q_x = 0$ state energy (blue dashed curves in Figure 2c), indicating an increase in the relative stability of the SS state. From the extracted result shown in Figure 2d (blue dashed curve), 5% compression and expansion lower the energy by ∼4.1 and ∼2.6 meV/f.u., respectively. Relative to the $q_x = 0.5$ state, the SS state becomes more energetically favorable for compressive strain but less stable for tensile strain. Therefore, compressive strain not only tunes the SS ordering wavevector but also increases the overall stability of the SS state.

Given that the SS we are considering is cycloidal, the electrical polarization is expected to be of the form $P \propto \hat{e} \times \boldsymbol{q}$, where $\hat{e}$ denotes the axis around which the spiral spins are rotating.[9] Therefore, in ML FeOCl, the unique $ac$-plane-constrained SS arrangement is expected to induce an out-of-plane polarization. As shown in Figure 3a, a clockwise spiral combined with a propagation vector along the positive $a$-axis induces a downward electronic polarization. The inverse-chirality SS is shown in Figure 3b with an upward electronic polarization. In contrast to the above, in layered materials with triangular lattices like $CuFeO_2$, the SS-induced polarization is in-plane.[34]

In order to calculate the electronic polarization induced by SS in ML FeOCl, the ground-state spiral vector must be


https://doi.org/10.1021/acs.nanolett.1c05043
Nano Lett. 2022, 22, 3598−3603

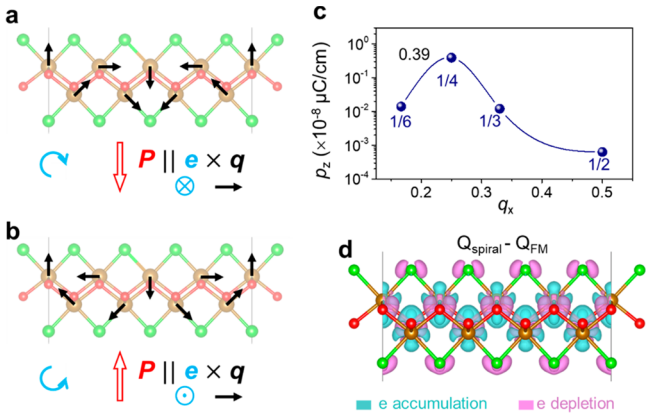


**Figure 3.** Multiferroicity of ML FeOCl. (a,b) Schematics showing how clockwise and anticlockwise SS arrangements generate an out-of-plane electric polarization in ML FeOCl. A 4 × 1 supercell is used. The energies of the states in panels a and b are the same. (c) Calculated out-of-plane polarization of ML FeOCl at distinct values of $q_x$. Values 1/6, 1/4, 1/3, and 1/2 correspond to the results with 6 × 1, 4 × 1, 3 × 1, and 2 × 1 supercells. (d) Charge density difference between the SS and FM states. Light blue/pink colors correspond to electron accumulation and depletion, respectively. The isosurface level is set as 4.7 × 10$^{-4}$ e/Å$^3$.

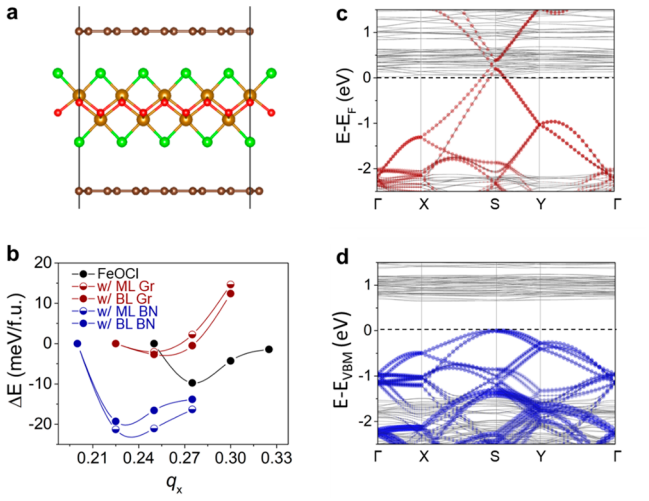


**Figure 4.** SS state of ML FeOCl in heterostructures. (a) Side view of schematic of ML FeOCl sandwiched by other 2D materials. Two-layers graphene are shown as prototype. (b) Energy−$q_x$ relationships of freestanding ML FeOCl (black), ML FeOCl stacking on ML graphene (red, half-open marks), ML FeOCl sandwiched in bilayer (BL) graphene (red, solid marks), ML FeOCl stacking on ML h-BN (blue, half-open marks), ML FeOCl sandwiched in BL h-BN (blue, solid marks), respectively. The Δ$E$ are referenced to the energy of the $q_x$ = 0 state. (c) Band structure of ML FeOCl sandwiched between two-layers graphene. Red curves indicate the projection on graphene. (d) Band structure of ML FeOCl sandwiched by two-layers h-BN. Blue curves indicate the projection on h-BN.

approximated using a supercell approach following established methodology.[35] The calculated polarization $\boldsymbol{P}$ has only a $P_z$ component, which is shown in Figure 3c as a function of $q_x$. A maximum value of 0.39 × 10$^{-8}$ $\mu$C/cm, is obtained when $q_x$ = 0.25, close to the calculated ground-state vector, $q_x$ = 0.274. Since the polarization arises from the inhomogeneity of the magnetization without the need for atomic displacements, the polarization value is referenced against a state with collinear magnetization, for example, the FM states. Comparison with other reported out-of-plane polarizations in layered materials indicates that the $p_z$ of ML FeOCl is an order of magnitude smaller than that of d1T-$MoTe_2$.[36] Looking for other materials with stronger polarization and researching the effects that strengthen the polarization, for example, stacking, remain open for future work.

To further examine the origin of the SS-induced electronic polarization, we examine the electron density redistribution by plotting the charge density difference between the SS and FM states in the 4 × 1 supercell. As shown in Figure 3d, the charge density of the upper surface row of Cl atoms is not equal to that of the lower surface row of Cl atoms. This SS-induced asymmetric charge redistribution is the origin of the out-of-plane polarization.

For many applications of 2D and layered materials, van der Waals heterostructures are often used to support/protect the inner materials and to assemble multifunctional devices. Therefore, we consider the effect of sandwiching a ML FeOCl between other 2D materials. Specifically, we considered the effects of using two prototypical monolayer materials, graphene and h-BN. Figure 4a illustrates the side view of a graphene/FeOCl/graphene heterostructure. In addition, we considered graphene/FeOCl and h-BN/FeOCl supported heterostructures (i.e., heterobilayers).

Figure 4b shows the variation of $q_x$ for ML FeOCl in each of the different heterostructures. Clearly, the SS ground state of the ML FeOCl persists in stacking heterostructures. For a graphene/FeOCl and a graphene/FeOCl/graphene heterostructure (red curves), the $q_x$ are smaller than the intrinsic value. For an h-BN/FeOCl and an h-BN/FeOCl/h-BN heterostructure (blue curves), the $q_x$ are also smaller than the intrinsic value. The heterostructure modulation implies that interface effects can provide an additional method to tune the SS state in ML FeOCl. It is notable that in the graphene-based heterostructures, the energy difference between the SS and $q_x$ = 0 states is smaller than in the freestanding ML, indicating that the SS state is now less stable. On the contrary, the energy difference is larger for h-BN heterostructures, indicating that h-BN makes the SS state more stable.

In order to understand how the heterostructures modify the SS propagation vector, we performed further analysis of their electronic structures. As shown in Figure 4c, graphene influences the SS state of FeOCl by doping. When FeOCl is encapsulated by two layers of graphene, the Fermi energy moves below the Dirac point of graphene and the conduction band minimum (CBM) of FeOCl sits slightly below the Fermi level, indicating that graphene is $p$-type doped while FeOCl is $n$-type doped. This behavior is consistent with the doping results shown in Figure 2a, that $n$-type doping shortens the SS propagation vector and decreases the energy difference. However, for h-BN, as shown in Figure 4d, the valence band maximum (VBM) of h-BN lies in the midgap region of FeOCl (i.e., Type II band alignment). Therefore, there is no electrostatic doping effect between FeOCl and h-BN. It is the orbital redistribution of FeOCl that results in a shortened SS propagation vector and increased energy difference (see details in Supporting Information).

In conclusion, we have shown that in the magnetic ground state, ML FeOCl possesses an *ac*-plane-constrained cycloidal spin spiral. In the ground state, the SS propagation vector is (0.274, 0.5, 0) and is highly tunable by electron/hole doping and uniaxial strain. Doping ML FeOCl $n$-type ($p$-type) causes a


https://doi.org/10.1021/acs.nanolett.1c05043
Nano Lett. 2022, 22, 3598−3603

decrease (increase) of $q_x$. In both cases, doping decreases the stability of the SS states. With $x$-direction uniaxial strain (i.e., strain along the propagation direction), compressive and tensile strain decreases and increases $q_x$, respectively. Both types of strain increase the stability of the SS state. An out-of-plane electron polarization originating from the spin spiral is confirmed. The cause of polarization is attributed to the asymmetric charge distribution in the SS state, which is a manifestation of the inhomogeneity of the magnetization. The SS state is sustained even when FeOCl forms supported or encapsulated heterostructures with graphene and h-BN. Graphene is found to tune FeOCl's spin spiral through electron doping, while orbital redistribution from the coupling between FeOCl and h-BN modulates the SS vector. The present discovery of SS in monolayer FeOCl paves the way to investigate spin-spiral coupling with ferroelectricity in monolayers, which may impact the development of magnetoelectric nanodevices with diversified functionalities, like switches, sensors, and inductors, at the two-dimensional level.

## ■ ASSOCIATED CONTENT

### Supporting Information

The Supporting Information is available free of charge at https://pubs.acs.org/doi/10.1021/acs.nanolett.1c05043.

Detailed computational methodology, exchange coupling and DMI parameters, phonon and lattice stability, additional electronic structure analysis of the Fe magnetic moments, quasi-one-dimensional model to analyze strength of $J$ versus $D$ in cycloidal spin spirals (PDF)

## ■ AUTHOR INFORMATION


### Corresponding Author

**Sokrates T. Pantelides** − *Department of Physics and Astronomy, Vanderbilt University, Nashville, Tennessee 37235, United States; Institute of Physics and University of the Chinese Academy of Sciences, Chinese Academy of Sciences, Beijing 100190, China; Department of Electrical and Computer Engineering, Vanderbilt University, Nashville, Tennessee 37235, United States;* orcid.org/0000-0002-2963-7545; Email: pantelides@vanderbilt.edu

### Authors

**De-Liang Bao** − *Department of Physics and Astronomy, Vanderbilt University, Nashville, Tennessee 37235, United States; Institute of Physics and University of the Chinese Academy of Sciences, Chinese Academy of Sciences, Beijing 100190, China;* orcid.org/0000-0002-5070-4765

**Andrew O'Hara** − *Department of Physics and Astronomy, Vanderbilt University, Nashville, Tennessee 37235, United States;* orcid.org/0000-0002-0323-9039

**Shixuan Du** − *Institute of Physics and University of the Chinese Academy of Sciences, Chinese Academy of Sciences, Beijing 100190, China;* orcid.org/0000-0001-9323-1307

Complete contact information is available at: https://pubs.acs.org/10.1021/acs.nanolett.1c05043

### Author Contributions

‖D.L.B and A.O. contributed equally to this work


### Notes

The authors declare no competing financial interest.

## ■ ACKNOWLEDGMENTS

This work was supported in part by the U.S. Department of Energy (DOE), Office of Science, Office of Basic Energy Sciences (BES), Materials Sciences and Engineering Division under Award DE-FG02-09ER46554 (A.O., S.T.P.), by the Vanderbilt McMinn Endowment (D.L.B., S.T.P.), and by the K. C. Wong Education Foundation of the Chinese Academy of Sciences (D.L.B., S.D.). Calculations were performed at the National Energy Research Scientific Computing Center (NERSC), a DOE Office of Science User Facility supported by the Office of Science of the U.S. Department of Energy under Contract No. DE-AC02-05CH11231 and by the Department of Defense's High-Performance Computing Modernization Program (HPCMP).

## ■ REFERENCES


(1) Pientka, F.; Glazman, L. I.; von Oppen, F. Topological superconducting phase in helical Shiba chains. *Phys. Rev. B* **2013**, *88* (15), 155420.

(2) Buessen, F. L.; Hering, M.; Reuther, J.; Trebst, S. Quantum spin liquids in frustrated spin-1 diamond antiferromagnets. *Phys. Rev. Lett.* **2018**, *120* (5), 057201.

(3) Takagi, H.; Takayama, T.; Jackeli, G.; Khaliullin, G.; Nagler, S. E. Concept and realization of Kitaev quantum spin liquids. *Nat. Rev. Phys.* **2019**, *1* (4), 264−280.

(4) Xu, C.; Chen, P.; Tan, H.; Yang, Y.; Xiang, H.; Bellaiche, L. Electric-Field Switching of Magnetic Topological Charge in Type-I Multiferroics. *Phys. Rev. Lett.* **2020**, *125* (3), 037203.

(5) Xu, C.; Feng, J.; Prokhorenko, S.; Nahas, Y.; Xiang, H.; Bellaiche, L. Topological spin texture in Janus monolayers of the chromium trihalides Cr(I, $X$)$_3$. *Phys. Rev. B* **2020**, *101* (6), No. 060404.

(6) Katsura, H.; Nagaosa, N.; Balatsky, A. V. Spin current and magnetoelectric effect in noncollinear magnets. *Phys. Rev. Lett.* **2005**, *95* (5), 057205.

(7) Kurumaji, T. Spiral spin structures and skyrmions in multiferroics. *Phys. Sci. Rev.* **2020**, *5* (1), 1−24.

(8) Xiang, H. J.; Kan, E. J.; Zhang, Y.; Whangbo, M. H.; Gong, X. G. General theory for the ferroelectric polarization induced by spin-spiral order. *Phys. Rev. Lett.* **2011**, *107* (15), 157202.

(9) Cheong, S. W.; Mostovoy, M. Multiferroics: a magnetic twist for ferroelectricity. *Nat. Mater.* **2007**, *6* (1), 13−20.

(10) Kimura, T.; Goto, T.; Shintani, H.; Ishizaka, K.; Arima, T.-h.; Tokura, Y. Magnetic control of ferroelectric polarization. *Nature* **2003**, *426* (6962), 55−58.

(11) Emori, S.; Bauer, U.; Ahn, S. M.; Martinez, E.; Beach, G. S. Current-driven dynamics of chiral ferromagnetic domain walls. *Nat. Mater.* **2013**, *12* (7), 611−616.

(12) Brataas, A. Spintronics: Chiral domain walls move faster. *Nat. Nanotechnol.* **2013**, *8* (7), 485−486.

(13) Kimura, T. Spiral magnets as magnetoelectrics. *Annu. Rev. Mater. Res.* **2007**, *37* (1), 387−413.

(14) Chen, G.; Ma, T.; N'Diaye, A. T.; Kwon, H.; Won, C.; Wu, Y.; Schmid, A. K. Tailoring the chirality of magnetic domain walls by interface engineering. *Nat. Commun.* **2013**, *4*, 2671.

(15) Hrabec, A.; Porter, N. A.; Wells, A.; Benitez, M. J.; Burnell, G.; McVitie, S.; McGrouther, D.; Moore, T. A.; Marrows, C. H. Measuring and tailoring the Dzyaloshinskii-Moriya interaction in perpendicularly magnetized thin films. *Phys. Rev. B* **2014**, *90* (2), 020402.

(16) Sessi, P.; Guisinger, N. P.; Guest, J. R.; Bode, M. Temperature and size dependence of antiferromagnetism in Mn nanostructures. *Phys. Rev. Lett.* **2009**, *103*, 167201.

(17) Hsu, P. J.; Finco, A.; Schmidt, L.; Kubetzka, A.; von Bergmann, K.; Wiesendanger, R. Guiding spin spirals by local uniaxial strain relief. *Phys. Rev. Lett.* **2016**, *116* (1), 017201.

(18) Steinbrecher, M.; Rausch, R.; That, K. T.; Hermenau, J.; Khajetoorians, A. A.; Potthoff, M.; Wiesendanger, R.; Wiebe, J. Non-

collinear spin states in bottom-up fabricated atomic chains. *Nat. Commun.* **2018**, *9* (1), 2853.
(19) Amoroso, D.; Barone, P.; Picozzi, S. Spontaneous skyrmionic lattice from anisotropic symmetric exchange in a Ni-halide monolayer. *Nat. Commun.* **2020**, *11* (1), 5784.
(20) Fumega, A. O.; Lado, J. L. Microscopic origin of multiferroic order in monolayer $NiI_2$. *2D Mater.* **2022**, *9* (2), 025010.
(21) Prayitno, T. B.; Ishii, F. First-principles study of spiral spin density waves in monolayer $MnCl_2$ using generalized Bloch theorem. *J. Phys. Soc. Jpn.* **2019**, *88* (10), 104705.
(22) Ding, N.; Chen, J.; Dong, S.; Stroppa, A. Ferroelectricity and ferromagnetism in a $VOI_2$ monolayer: Role of the Dzyaloshinskii-Moriya interaction. *Phys. Rev. B* **2020**, *102* (16), 165129.
(23) Laref, S.; Kim, K.-W.; Manchon, A. Elusive Dzyaloshinskii-Moriya interaction in monolayer $Fe_3GeTe_2$. *Phys. Rev. B* **2020**, *102* (6), 060402.
(24) Zhang, J. J.; Lin, L. F.; Zhang, Y.; Wu, M. H.; Yakobson, B. I.; Dong, S. Type-II Multiferroic $Hf_2VC_2F_2$ MXene Monolayer with High Transition Temperature. *J. Am. Chem. Soc.* **2018**, *140* (30), 9768−9773.
(25) Hwang, S. R.; Li, W.-H.; Lee, K. C.; Lynn, J. W.; Wu, C.-G. Spiral magnetic structure of Fe in Van der Waals gapped FeOCl and polyaniline-intercalated FeOCl. *Phys. Rev. B* **2000**, *62* (21), 14157.
(26) Adam, A.; Buisson, G. Structure magnétique cycloïdale de FeOCl. *Phys. Status Solidi A* **1975**, *30* (1), 323−329.
(27) Ferrenti, A. M.; Klemenz, S.; Lei, S.; Song, X.; Ganter, P.; Lotsch, B. V.; Schoop, L. M. Change in magnetic properties upon chemical exfoliation of FeOCl. *Inorg. Chem.* **2020**, *59* (2), 1176−1182.
(28) Bonacum, J. P.; O'Hara, A.; Bao, D.-L.; Ovchinnikov, O. S.; Zhang, Y.-F.; Gordeev, G.; Arora, S.; Reich, S.; Idrobo, J.-C.; Haglund, R. F.; et al. Atomic-resolution visualization and doping effects of complex structures in intercalated bilayer graphene. *Phys. Rev. Mater.* **2019**, *3* (6), 064004.
(29) Jin, X.; Zhang, Y.-Y.; Pantelides, S. T.; Du, S. Integration of graphene and two-dimensional ferroelectrics: properties and related functional devices. *Nanoscale Horiz.* **2020**, *5* (9), 1303−1308.
(30) Gong, C.; Kim, E. M.; Wang, Y.; Lee, G.; Zhang, X. Multiferroicity in atomic van der Waals heterostructures. *Nat. Commun.* **2019**, *10* (1), 1−6.
(31) Lu, Y.; Fei, R.; Lu, X.; Zhu, L.; Wang, L.; Yang, L. Artificial multiferroics and enhanced magnetoelectric effect in van der Waals heterostructures. *ACS Appl. Mater. Interfaces* **2020**, *12* (5), 6243−6249.
(32) Sun, W.; Wang, W.; Chen, D.; Cheng, Z.; Wang, Y. J. N. Valence mediated tunable magnetism and electronic properties by ferroelectric polarization switching in 2D $FeI_2/In_2Se_3$ van der Waals heterostructures. *Nanoscale* **2019**, *11* (20), 9931−9936.
(33) Deng, S.; Sumant, A. V.; Berry, V. Strain engineering in two-dimensional nanomaterials beyond graphene. *Nano Today* **2018**, *22*, 14−35.
(34) Zhang, J. T.; Ji, C.; Wang, J. L.; Xia, W. S.; Guo, B. X.; Lu, X. M.; Zhu, J. S. Spin-induced ferroelectricity in a triangular-lattice antiferromagnet studied by magnetoelectric coupling tensors. *Phys. Rev. B* **2017**, *96* (23), 235136.
(35) Xiang, H. J.; Whangbo, M. H. Density-functional characterization of the multiferroicity in spin spiral chain cuprates. *Phys. Rev. Lett.* **2007**, *99* (25), 257203.
(36) Yuan, S.; Luo, X.; Chan, H. L.; Xiao, C.; Dai, Y.; Xie, M.; Hao, J. Room-temperature ferroelectricity in $MoTe_2$ down to the atomic monolayer limit. *Nat. Commun.* **2019**, *10* (1), 1775.





https://doi.org/10.1021/acs.nanolett.1c05043
*Nano Lett.* 2022, 22, 3598−3603